

Electrochemical Growth of Micrometer-Thick Oxide on SiC in Acidic Fluoride Solution

D.H. van Dorp,^{*,†} E.S. Kooij,[‡] W.M. Arnoldbik,[†] and J.J. Kelly[†]

[†]Debye Institute for NanoMaterials Science, Utrecht University, Princetonplein 1, 3584 CC, Utrecht, The Netherlands, and [‡]Solid State Physics, MESA+ Research Institute, University of Twente, P.O. Box 217, 7500 AE Enschede, The Netherlands

Received March 25, 2009. Revised Manuscript Received June 12, 2009

Anodic polarization of SiC at modest potential in dilute fluoride solution of pH 3 surprisingly gives rise to the growth of micrometer-thick surface layers, clearly revealed with scanning electron microscopy. The reaction occurs at p-type SiC in the dark and at n-type SiC under (supra)bandgap illumination. The surface layer was shown by Rutherford backscattering spectrometry (RBS) to consist of silicon dioxide and to contain excess oxygen. Elastic recoil detection (ERD) indicated only a low level of carbon and fluoride in the layer but a considerable content of hydrogen. The growth kinetics was characterized in situ by spectroscopic ellipsometry and electrical impedance spectroscopy. The results suggest the formation of a duplex layer: a thin inner dielectric oxide and a thick hydrated outer oxide. The latter must have a considerable degree of porosity to allow diffusion/migration of reactants and products during oxide growth.

1. Introduction

The wide-bandgap, chemically resistant semiconductor SiC is finding application in a broad range of fields: microelectronics, microelectromechanical systems [MEMS], sensors, and biomedical systems.^{1–3} In such applications, etching of the semiconductor is often an essential step. Anodic dissolution offers an attractive alternative to dry etching methods.⁴ To dissolve SiC electrochemically, one must, as in the case of Si, limit passivation caused by oxide growth. This implies the use of electrolyte solutions in which SiO₂ shows a considerable solubility. In previous work, we described the anodic dissolution and passivation of SiC in KOH solution.^{5,6} There is already a considerable literature on the electrochemistry of SiC in acidic fluoride solution. The emphasis has been on the (photo)electrochemical dissolution, including porous etching.^{7–12} Most of the work has been performed at rather high fluoride concentration, at current densities for which oxide formation is not

significant. Strikingly, under similar conditions, anodic oxide is formed on Si.^{13,14} The reason for this difference between the two semiconductors is of fundamental interest; in addition, anodic oxide on SiC has interesting potential applications.

The current–potential characteristics of p-type Si (and n-type Si illuminated at high light intensity) in acidic fluoride solution show three main ranges. In the onset of the current, the surface is hydrogen terminated and porous etching occurs. At more positive potential, a peak in the voltammogram followed by a plateau indicates a change in surface chemistry. The hydride is converted to hydroxide and an oxide grows; the semiconductor is electropolished in this range. The appearance of a second peak is due to the growth of a complex oxide. This has been the subject of considerable study, especially because it gives rise to interesting current oscillations.^{15–17} Electrical impedance shows the presence of a thin barrier oxide (3 nm), whereas ellipsometry reveals a thicker oxide (up to 30 nm). Bailes and co-workers distinguish an inner layer of “dry” oxide and a thicker outer layer of hydrated oxide.¹⁸ In situ infrared spectroscopic measurements confirm the complexity of the surface oxide.¹⁹

*Corresponding author. E-mail: D.H.vanDorp@uu.nl.

- (1) Neudeck, P. G. *SiC Technology*; CRC Press: Boca Raton, FL, 2000.
- (2) Sarro, P. M. *Sens. Actuators, A* **2000**, *82*, 210.
- (3) Rosenbloom, A. J.; Sipe, D. M.; Shishkin, Y.; Ke, Y.; Devaty, R. P.; Choyke, W. J. *Biomed. Dev.* **2004**, *6*, 261.
- (4) Notten, P. H. L.; van den Meerakker, J. E. A. M.; Kelly, J. J. *Etching of III-V Semiconductors*; Elsevier Advanced Technology: Oxford, U.K., 1991.
- (5) van Dorp, D. H.; Kelly, J. J. *J. Electroanal. Chem.* **2007**, *599*, 260.
- (6) van Dorp, D. H.; Weyher, J. L.; Kelly, J. J. *J. Micromech. Microeng.* **2007**, *17*, S50.
- (7) Shor, J. S.; Grimberg, I.; Weiss, B. Z.; Kurtz, A. D. *Appl. Phys. Lett.* **1993**, *62*, 2836.
- (8) Shor, J. S.; Osgood, R. M. *J. Electrochem. Soc.* **1993**, *140*, L123.
- (9) Shor, J. S.; Kurtz, A. D. *J. Electrochem. Soc.* **1994**, *141*, 778.
- (10) Shor, J. S.; Zhang, X. G.; Osgood, R. M. *J. Electrochem. Soc.* **1992**, *139*, 1213.
- (11) Zangoie, S.; Persson, P. O. A.; Hilfiker, J. N.; Hultman, L.; Arwin, H. *J. Appl. Phys.* **2000**, *87*, 8497.
- (12) Zangoie, S.; Arwin, H. *Phys. Status Solidi A* **2000**, *182*, 213.

- (13) Chazalviel, J. N.; Etman, M.; Ozanam, F. *J. Electroanal. Chem.* **1991**, *297*, 533.
- (14) Hassan, H. H.; Sculfort, J. L.; Etman, M.; Ozanam, F.; Chazalviel, J. N. *J. Electroanal. Chem.* **1995**, *380*, 55.
- (15) Chazalviel, J. N.; Ozanam, F.; Etman, M.; Paolucci, F.; Peter, L. M.; Stumper, J. *J. Electroanal. Chem.* **1992**, *327*, 343.
- (16) Chazalviel and, J. N.; Ozanam, F. *J. Electrochem. Soc.* **1992**, *139*, 2501.
- (17) Chazalviel, J. N.; da Fonseca, C.; Ozanam, F. *J. Electrochem. Soc.* **1998**, *145*, 3312.
- (18) Bailes, M.; Bohm, S.; Peter, L. M.; Riley, D. J.; Greef, R. *Electrochim. Acta* **1998**, *43*, 1757.
- (19) daFonseca, C.; Ozanam, F.; Chazalviel, J. N. *Surf. Sci.* **1996**, *365*, 1.

We showed that at lower fluoride concentration there is a similarity in the electrochemistry of Si and SiC, although the current density in the case of the compound semiconductor is markedly higher than that of Si under similar conditions.^{20,21} In this work, we focus on the potential range in which a complex oxide is formed. In situ electrochemical measurements (voltammetry and electrical impedance) were supported by in situ spectroscopic ellipsometry. In addition, the surface layer formed was studied ex situ by scanning electron microscopy (SEM), Rutherford backscattering spectrometry and elastic recoil detection. We found that extremely thick, coherent oxide layers (up to 5 μm) can be grown on SiC in dilute fluoride solution. Relatively high anodic current densities are observed, indicating a high permeability of ions and water in the oxide. This suggests porosity at the molecular level. We speculate on the mechanism of oxide formation.

There have been previous reports of anodic oxide growth on SiC. Lauer mann et al.²² describe the formation of a thick white layer of silicon oxides on p-type SiC (in the dark) and n-type SiC (under illumination) after prolonged current flow in H_2SO_4 solution. The layer readily dissolved in HF solution. Gaseous products, CO and CO_2 , were formed in equal amounts during oxidation. Shor et al.¹⁰ also observed oxide formation on UV-laser illumination of n-type β -SiC in 0.5 M H_2SO_4 solution. The layer was 20 nm thick and had a low carbon content (< 3%). They describe the oxide as “nonpassivating”, suggesting that it was sufficiently “porous” to allow the electrolyte to stay in contact with the semiconductor surface. Rysy et al.,²³ in an appendix to a paper on the electrochemical etching of SiC, describe the growth of micrometer-thick SiO_2 on n-type 6H-SiC, under illumination in 0.2 M HCl solution at positive potential. RBS and profilometry were used to characterize the oxide. The surface of the oxide was rough and showed cracks, attributed by the authors to volume expansion of the layer. Oxide growth on SiC in solutions of H_2SO_4 and HCl is not unexpected (the oxide solubility is low), although the extremely thick layer reported by Rysy et al. is surprising. The growth of equally thick oxide on SiC in acidic fluoride solution may, on the basis of a comparison with Si, be considered even more surprising.

2. Experimental Section

Single-crystal p-type 4H-SiC and n-type 4H and 6H-SiC wafers were obtained from Cree (United States). The p-type wafer was oriented 8° off-axis and aluminum-doped, and had a resistivity of 3.86 Ω cm. The n-type wafers were on-axis and nitrogen-doped and had a resistivity of 0.06–0.07 Ω cm.

All wafers used in this study were Si terminated. A circular exposed area was defined on the samples by a Si_3N_4 mask. The diameter of the opening was 2 mm. Ohmic contacts to the p-type SiC were made by evaporating a 300 nm thick layer of Al/Ta/Au on the back side of the wafer. The metallized wafer was subsequently annealed at 850 °C for 10 min. The n-type wafers were contacted by depositing a 300 nm Ti/Au layer followed by a 1 s annealing step at 1000 °C.

The fluoride solutions were prepared from analytical grade NH_4F and HF solutions and deionized water (Millipore 18 M Ω cm) and were buffered at a pH of 3.^{13,14,24} The pH was determined by pH indicators and the ionic strength of the solution was set at 1 M by addition of NH_4Cl .

Measurements were performed in a conventional three-electrode cell with a platinum counter electrode and a saturated calomel electrode (SCE) as a reference; potentials are given with respect to SCE. To prevent attack by the etchant, we placed the reference electrode in a separate compartment connected to the main cell via a salt bridge. A potentiostat (EG&G Princeton Applied Research, PAR-273-A), computer-controlled by LabVIEW, was used to measure the current–potential curves. To study the influence of mass transport on the system, we mounted the samples as a rotating disk electrode (RDE). During the measurements, the temperature was kept at 21 ± 0.5 °C. Oxide on n-type SiC was grown under illumination from a 450W Hg/Xe arc lamp (Oriel 66924). Electrochemical impedance was studied with a Schlumberger SI 1255 HF frequency response analyzer, computer-controlled by LabVIEW. For measurement of the Nyquist plots, the frequency was varied from 50 Hz to 50 kHz. Each plot took 30 s. Two types of experiment were performed: transient measurements after a potential step and quasi-steady-state measurements at fixed potential as a function of electrode rotation rate.

Two ion-beam analysis techniques, Rutherford backscattering spectrometry (RBS) and elastic recoil detection (ERD), were applied to determine the composition of the films as well as the atomic areal density in at/cm^2 . Both techniques are based on binary elastic collisions and employ ion beams with an energy in the order of 1 MeV per nucleus. RBS, used to measure the O/Si ratio and the areal density of the oxide layers, uses light projectiles, in this case 2 MeV He^+ ions. The energy of ions (back)scattered over an angle of 170° was analyzed by a solid-state detector. ERD was used to determine the hydrogen concentration and upper limits for the carbon and fluorine concentration in the oxide layers and is complementary to RBS; here, heavy ions (50 MeV Cu^{8+}) were used and atoms recoiled from the target were detected under a forward angle of 30°. For the detection and identification of the recoiled particles a gas-filled ΔE – E ionization chamber, equipped with a solid-state stop-detector for the detection of hydrogen recoils, was used. Both techniques give depth-resolved compositional information, based on the stopping power that both the incoming and the outgoing ions experience during their traverse through the sample.

For the optical experiments, a Woollam variable angle spectroscopic ellipsometer (VASE) system was used. Measurements were performed either at a fixed photon energy of 2.5 eV or as a function of photon energy in the range 1.5–4.5 eV. The advantage of the former is that it allows more rapid measurement, typically 80 samples per minute. Spectral measurements are considerably slower; typically, a step size of 0.1 eV is used,

(20) van Dorp, D. H. Etching of wide-bandgap chemically resistant semiconductors—an electrochemical study. PhD Thesis, Utrecht University, Utrecht, The Netherlands, **2008**.

(21) van Dorp, D. H.; Sattler, J. J. H. B.; den Otter, A.; Kelly, J. J. *Electrochim. Acta* **2009**, in press.

(22) Lauer mann, I.; Memming, R.; Meissner, D. *J. Electrochem. Soc.* **1997**, *144*, 73.

(23) Rysy, S.; Sadowski, H.; Helbig, R. *J. Solid State Electrochem.* **1999**, *3*, 437.

(24) Etman, M.; Neumannspallart, M.; Chazalviel, J. N.; Ozanam, F. J. *Electroanal. Chem.* **1991**, *301*, 259.

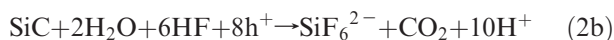
which gives approximately 8 spectra every 10 min. For the in situ ellipsometry measurements, a dedicated electrochemical cell was used. Optical access to the sample, mounted in the cell on a removable holder, was achieved through two windows at a fixed angle of incidence θ of 63° , close to the Brewster angle of SiC in contact with an aqueous solution. A third window allowed alignment of the sample at normal incidence and visual inspection of the sample during in situ experiments. In reflection ellipsometry, the change in the polarization state of linearly polarized light is measured upon reflection at an interface. The complex reflection coefficient ρ is defined as

$$\rho = \frac{r_p}{r_s} = \tan(\Psi)\exp(i\Delta) \quad (1)$$

where r_p and r_s are the reflection coefficients for the parallel and perpendicular polarizations, respectively. Historically, the quantity ρ is expressed in two angles Ψ and Δ .²⁵ Although the actual ellipsometry measurement is relatively simple, the analysis of the results is often complicated. Generally an accurate model is required to enable simulation or fitting of the results. Unfortunately, we were not able to adequately describe the optical characteristics of SiC in contact with the aqueous electrolyte using a straightforward model. As we were primarily interested in the formation and dissolution of the interfacial layer, we chose a simple procedure to determine film thickness from the ellipsometry spectra. The thickness d was such that the spectra exhibited oscillations as a function of photon energy due to interference of light reflected from the film/substrate and the liquid/film interfaces. The path length difference of light reflected at these interfaces amounts to $2nd\cos(\beta)$, where n is the dielectric constant of the film relative to that of the liquid in contact with it: $n = n_{\text{film}}/n_{\text{water}}$. The angle β of the light beam in the film is related to the angle of incidence via Snell's law $n_{\text{water}}\sin(\theta) = n_{\text{film}}\sin(\beta)$. For constructive interference, the optical path length should be equal to a whole number of wavelengths, whereas destructive interference occurs when the path lengths differ by half a wavelength. A plot of the energy positions of subsequent maxima (or minima) yields a straight line. The slope is inversely proportional to the thickness of the film.

3. Results

3.1. Electrochemistry. In Figure 1, electrochemical results are presented for 4H-SiC electrodes in 0.033 M fluoride solution at pH 3. Figure 1a shows cyclic voltammograms for a p-type RDE at a rotation rate of 100 rpm. The potential was scanned from 1.75 V to 4.0 V and back at scan rates ranging from 2.5 to 40 mV/s. In the potential range in which the current density increases exponentially, anodic dissolution of the semiconductor occurs. This requires either 6 or 8 valence-band holes per SiC formula unit²¹



and gives a hexafluoride complex in solution and CO or CO₂. Gas evolution was observed in the whole range of

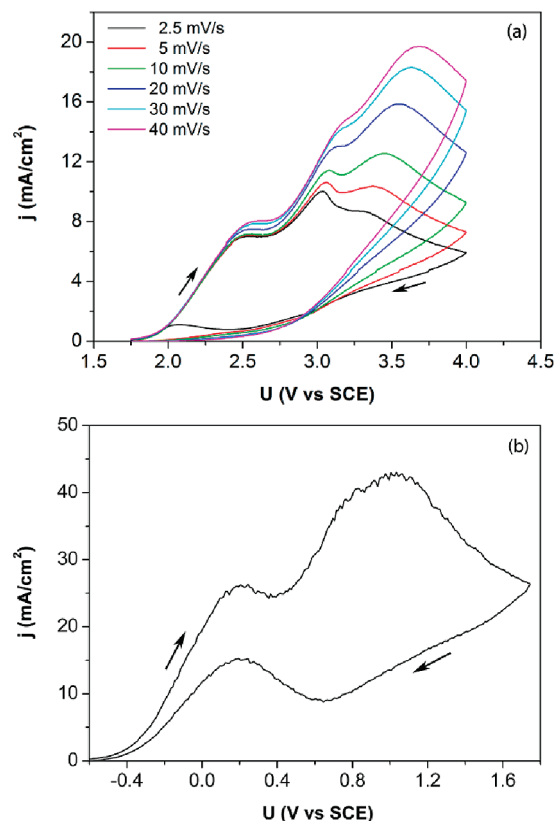
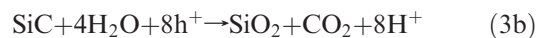
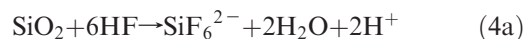


Figure 1. Current density–potential plots for 4H-SiC in 0.033 M fluoride solution (pH 3) at 100 rpm: (a) influence of potential scan rate for p-type 4H-SiC electrode in the dark and (b) n-type 4H-SiC under illumination at a potential scan rate of 10 mV/s.

the voltammogram. The occurrence of a current plateau signals a change in surface chemistry from an oxide-free to a (partly) blocked surface. SiC is also dissolved in this range; the dissolution rate is determined by mass transport, as is clear from a strong dependence on the electrode rotation rate.²¹ (As shown elsewhere,²¹ this dependence can be described by a Koutecky–Levich analysis, indicating mixed kinetic/mass transport control.) At more positive potential the current goes through a maximum for all scan rates. The considerable hysteresis in the return scan indicates the formation of a blocking layer which, as will be shown, consists of SiO₂. In analogy to eq 2a and 2b, this process could be represented by



However, the structure in the voltammograms suggests that a complex oxide may be involved. The strong influence of potential scan rate in this range shows oxide formation to be relatively slow. For the lowest scan rate (2.5 mV/s), the anodic current recovers at the end of the reverse scan. The oxide, obviously, dissolves slowly in a chemical reaction involving HF or HF₂^{-13,26}



(25) Azzam, R.M.A.; Bashara, N.H.; Ellipsometry and Polarized Light; North Holland: Amsterdam, 1987.

(26) Judge, J. S. *J. Electroanal. Chem.* **1971**, *118*, 1772.

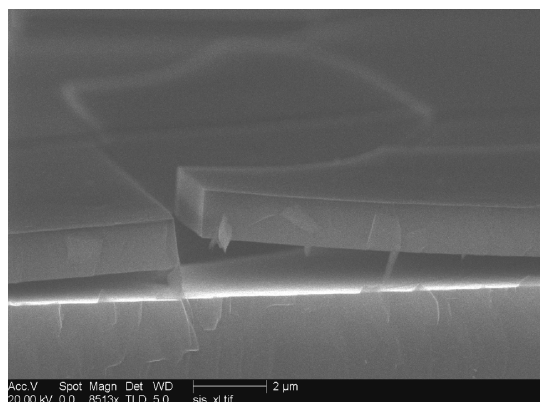


Figure 2. Side view of an anodic oxide layer grown on n-type 6H-SiC in a 3.3 mM fluoride solution of pH 3 under illumination. The SEM image was taken after a potential scan from -0.5 V to 3 V at a scan rate of 10 mV/s.



Clearly, for the conditions of Figure 1a, the rate of oxide dissolution is low compared to the rate of anodic oxide formation. It would have been instructive to measure quasi-reversible voltammograms. However, for the low fluoride concentrations of interest in this work, the establishment of steady-state conditions is painstakingly slow (see also section 3.3). Impractical scan rates would have been required. The current density in the passive range depends on the electrode rotation rate, though less strongly than in the current plateau.²¹

For anodic oxidation of the n-type semiconductor, valence-band holes must be generated by (supra)bandgap illumination. Figure 1b shows a cyclic voltammogram for the 4H-SiC electrode at relatively high light intensity. The general form of the current–potential curve resembles that of p-type SiC, showing that the surface chemistry is similar. There is, however, one striking difference between the two electrodes. In the onset of the photocurrent, anodic etching of n-type SiC gives rise to a macroporous structure. (At low light intensity, porosity is observed in the whole potential range.) The p-type electrode does not become porous. Porosity is responsible for the higher (geometric) current density required to passivate the n-type SiC in the scan to positive potential.²¹

3.2. Ex situ Characterization of Surface Layer.

The surface layers grown on p-type SiC in the dark and on n-type SiC under illumination were examined with SEM. A cross-section of a layer on an n-type electrode is shown in Figure 2. During cleaving, the oxide detached from the substrate and fractured. It is clear that a flat, coherent film has been formed with a thickness of about 1.3 μm . A similar result was found for the p-type electrode oxidized in the dark.

Figure 3 shows the RBS spectrum of an anodic layer formed on p-type 4H-SiC at 4.5 V. The RUMP simulation reveals an O/Si ratio of 2.3 ± 0.05 and a total of 7370×10^{15} silicon and oxygen atoms per cm^2 . A similar spectrum was obtained for the layer formed on the n-type electrode. Because hydrogen atoms are lighter than the

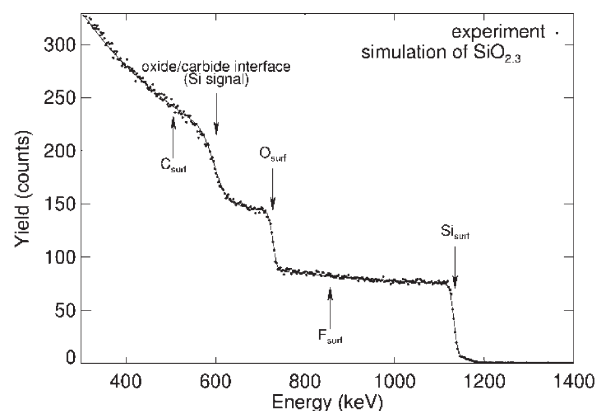


Figure 3. RBS spectrum of an anodic oxide layer grown on p-type 4H-SiC. The solid line represents a simulation of a layer with a O/Si ratio of 2.3 and an areal density of 7370×10^{15} Si+O at/ cm^2 on SiC. The energies corresponding to the surface for carbon, oxygen, fluorine and silicon are indicated, as well as the energy at which the Si concentration increases as a function of depth due to the interface with the substrate.

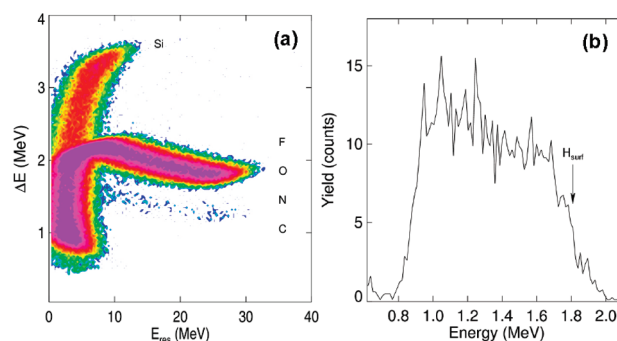


Figure 4. (a) ERD spectrum of an anodic oxide layer on p-type 4H-SiC measured with the ΔE – E ionization chamber. Indicated are the positions where features corresponding to relevant elements are expected. Probing depth for C, O, and F is about 0.5 μm . (b) Hydrogen spectrum.

He projectiles, they cannot be detected by RBS. RBS is also not suitable for detecting low concentrations of C and F, because their contribution to the spectrum is concealed by the huge Si and O features.

Figure 4a shows an example of an ERD ΔE – E spectrum measured with the ionization chamber. Clearly visible is a carbon signal which most likely does not originate from the oxide layer itself but from Cu ions that accidentally hit carbon-containing material surrounding it. Therefore, we interpret the carbon concentration of ~ 0.1 at % corresponding to this spectrum as an upper limit for the actual carbon concentration in the oxide. This indicates that there is very little elementary carbon in the layer and that CO and CO₂ (eq 2a) are removed under the high-vacuum conditions of the ERD experiment. The sensitivity for F is limited by the incomplete separation between O and F features. Here also we have to present an upper limit which amounts to 0.05 at%. These results show the passivating layer to be SiO₂. The hydrogen spectrum, measured with the stop detector at the rear end of the ionization chamber is depicted in Figure 4b. The hydrogen concentration in all oxide layers amounted to about 10 at %. The detection of a considerable amount of hydrogen in the layer together with excess oxygen

indicates the presence of hydroxyl species and strongly bound water. Weakly bound water will be removed during the RBS/ERD measurements.

3.3. In situ Characterization and Kinetics of Oxide Growth. Ellipsometry measurements were performed under potentiodynamic control to monitor the thickness changes of the passivating layer. Results of a typical experiment are shown in Figure 5. The potential was scanned from 1.5 to 4.5 V and back to 1.5 V at a rate of 2 mV/s in 0.033 M fluoride solution (pH 3). The current density and ellipsometric parameters were measured simultaneously. The solution was not stirred. For convenience, the potential axis is converted to a time scale. Figure 5a shows the current density as a function of time (i.e., potential) with a contour plot of the ellipsometric Ψ spectra as background. In the forward scan, the current density increases after 3.3 min (1.75 V) and a peak with a current density of about 1.5 mA/cm² is observed. During this initial current feature, no optical changes are detected, indicating that no significant oxide growth occurs. The subsequent current rise after 8.3 min (2.50 V) is accompanied by a marked change of Ψ (and Δ , not shown), over the entire spectral range, indicating a major change at the electrode surface. The current density peaks at approximately 15 min (3.18 V) and subsequently decreases gradually, which indicates the formation of a passivating layer on the electrode surface. The optical signals exhibit relatively rapid oscillations as a function of photon energy, which we ascribe to the thickness increase of the layer. Figure 5b shows results for ψ at a photon energy of 2.5 eV. Interference of light reflected at the solution-oxide and at the oxide-substrate interfaces gives rise to maxima and minima in ψ and Δ . Qualitatively, the time difference between two subsequent maxima (or minima) corresponds to an increase (or a decrease) of the thickness by approximately half the wavelength of the light. When the scan direction is reversed at 25 min (4.5 V), the current decreases slowly, then more rapidly and vanishes at the end of the scan (at 50 min). After the current maximum, the time separation between optical extremes becomes larger, indicating a slower change in oxide thickness. Long after the potential scan is finished, the oscillations persist, indicating that the thickness of the oxide layer is still changing. The observed decrease of ψ (and Δ) values at the maxima and minima in Figure 5b is ascribed to a roughening of the surface; indeed, visual inspection of the electrode after prolonged scanning reveals significant diffuse scattering due to surface roughness with length ranges in the order of the wavelength of the light.

The energy positions of the maxima and minima can be used to determine the oxide thickness, as described in the Experimental Section. The refractive index of the film is taken to be that of SiO₂, $n_{\text{film}} = 1.47$. (Using the Bruggeman effective-medium model and a value of 1.33 for the refractive index of the aqueous solution in the pores we expect a change of 2% in the refractive index of the layer for a porosity of 20%). The calculated thickness is plotted, together with current density, as a function of

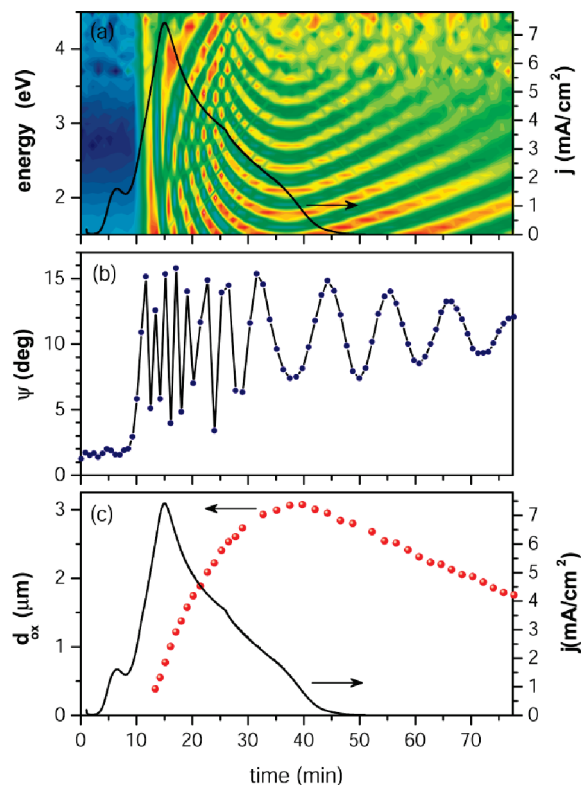


Figure 5. Electrochemical and ellipsometric measurements for a p-type 4H-SiC electrode in 0.033 M fluoride solution at pH 3. (a) Current density as a function of time for a potential scan from 1.5 to 4.5 V and back to 1.5 V (scan rate 2 mV/s). A contour plot of the ellipsometric Ψ spectra is shown as background in this figure. (b) The time-dependence of the ellipsometric parameter Ψ was obtained at fixed photon energy of 2.5 eV. (c) The oxide thickness determined from the ellipsometric data, as a function of time. For comparison, the voltammogram is also shown.

time in Figure 5c. As already concluded above, an oxide layer only starts to grow when the current increases beyond the first peak. After the current maximum, the current density decreases, whereas the oxide thickness continues to increase, as can be expected because charge is still being transferred across the solid-solution interface. Even after the potential scan direction is reversed, the oxide continues to grow, until a maximum thickness of 3 μm is reached at approximately 38 min; this is remarkably large considering the rather large current passing through the layer. The thickness maximum in Figure 5c corresponds to a shoulder in the current density-time plot during the reverse scan, after which the current density starts to decrease more rapidly to zero. In this range, the oxide thickness decreases at an approximately constant rate of 36 nm/min; this rate corresponds to what we expect on the basis of mass-transport control by HF and HF₂⁻. The very high etch rate, compared to that of thermal oxide,^{18,26} indicates that the passivating layer must be considerably less compact. The etching of the passivating layer continues after the end of the potential scan, when the electrode is again at open circuit. Experiments at different fluoride concentrations confirm that the etch rate depends on the solution composition. For example, when we increased the fluoride concentration from 0.033 to 0.1 M at pH 3, the etch rate increased by a

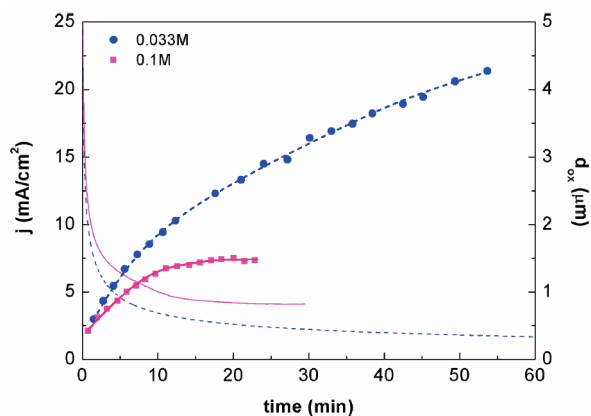


Figure 6. Time dependence of the oxide thickness (symbols, right-hand axis), as determined from ellipsometry spectra, and the simultaneously measured current density (lines, left-hand axis), after the potential of a p-type 4H-SiC electrode was stepped from open circuit to 4.5 V. Measurements were performed in 0.033 M (dotted lines) and 0.1 M fluoride (solid lines) solutions of pH 3.

factor of 4.4. Forced convection by stirring the solution in the cell also lead to a considerable increase of the etch rate, indicating that dissolution is diffusion-controlled. The time required to regain the initial, oxide-free surface is reduced at higher stirring rates.²⁰

During the entire oxidation process there is clearly a competition between electrochemical growth and chemical etching of the oxide. The latter depends on the fluoride concentration and mass transport, while the former is determined by the anodic current density. As soon as the oxide starts to grow after 8.3 min, it is also etched back. As long as the growth rate is larger than the etch rate, the overall thickness increases. Only when the formation rate becomes smaller than the etch rate (at approximately 38 min) does the constant etch rate “win”, giving rise to a decrease of the layer thickness. These ideas are confirmed by transient measurements following a potential step. The results of two experiments are shown in Figure 6, for a p-type electrode in 0.033 and 0.10 M fluoride solutions at pH 3. After the potential is stepped from open circuit to 4.5 V, a relatively large current is initially measured; this decreases rapidly as oxide is formed. As expected, the higher fluoride concentration indeed leads to a more rapid saturation of the anodic current at a value higher than that for the lower concentration. Accordingly, in solution with a higher HF concentration, the larger etch rate leads to a slower increase of the layer thickness, and also to a lower steady-state thickness of 1.5 μm . (The steady-state is established within 10–15 min.) Surprisingly, in the experiments in 0.033 M fluoride solution, a constant thickness was not reached in the time scale of the experiment (60 min). Oxide layers up to 4.3 μm thick have been observed after 54 min of oxidation (Figure 6), and thicker layers are possible. It is interesting to note that this oxide thickness is more than 3 orders of magnitude larger than that obtained on Si under comparable conditions.¹⁸ As described above, prolonged oxidation eventually leads to an optically rough SiC surface, thereby inhibiting ellipsometry measurements.

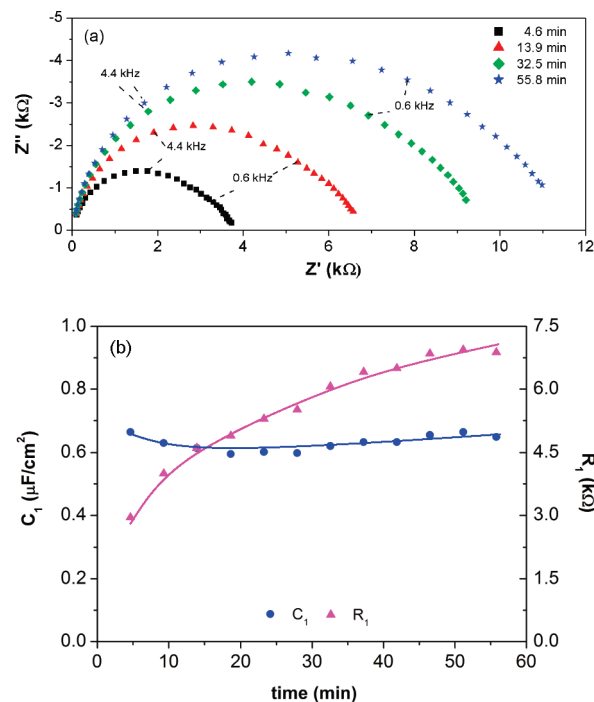


Figure 7. (a) Impedance spectra (Nyquist plots) were recorded for a p-type 4H-SiC electrode in 0.033 M fluoride solution (pH 3) at various times after a potential step from open-circuit to +3.5 V (frequency range 50 Hz to 50 kHz). The time indicated corresponds to the first frequency (50 Hz). (b) Time dependence of C_1 and R_1 derived from the fit of the measured impedance values.

The growth of thick oxide layers on n-type SiC illuminated at high light intensity was also confirmed by ellipsometry.

3.4. Impedance Spectroscopy. The electrical impedance of a stationary p-type SiC electrode in 0.033 M fluoride solution of pH 3 was measured in the potential range of oxide growth. Results in the form of Nyquist plots are shown in Figure 7a for various times after the potential was stepped from open circuit to 3.5 V. The imaginary component of the impedance Z'' is plotted as a function of the real component Z' for frequencies ranging from 50 Hz to 50 kHz. A somewhat flattened “semicircle” comprising at least two contributions is observed for all four times shown. The radius of the semicircle increases markedly from about 3500 Ω to 11500 Ω in 56 min. The spectra could be fitted satisfactorily by a simple $R_0(R_1/Q_1)(R_2/Q_2)$ circuit: a series connection of two parallel RQ circuits and a series resistance (Q is a constant phase element (CPE)). The series resistance R_0 , which can be attributed to the bulk semiconductor, the Ohmic contact and the electrolyte, is in all cases quite low ($\sim 15 \Omega$). The value of the CPE exponent n for the “high frequency circuit” (R_1/Q_1) is 0.95, which is close to the value of 1 expected for a capacitance. The value of n for Q_2 was markedly lower than 1 (an average of 0.85), indicating deviation from a capacitance. The value of Q_2 was considerably larger than that of Q_1 (by a factor of 20–30). It should be noted that on the time scale of these measurements (30 s) the system is not “stable”. Figure 6 shows that following a potential step, the current and oxide thickness change quite significantly at shorter times and then more slowly.

However, for times longer than 4 min, as shown in Figure 7, the shape of the Nyquist plots is very similar (this also holds for the experiments described below for different rotation rates). The parameters derived from the fits may deviate somewhat from their true values because of the finite measurement time. However, we are convinced that the trends observed are reliable.

Figure 7b shows the time dependence of Q_1 (plotted as a capacitance C_1) and R_1 , derived from the fit of the measured impedance values. The resistance R_1 increases from about 3000 Ω to 7000 Ω , whereas the capacitance remains constant at 0.6 $\mu\text{F}/\text{cm}^2$. Because the capacitance C_1 is close to that found for the anodic “dry” oxide on Si,^{18,27,28} it seems likely that the high-frequency impedance observed here for SiC is due to barrier oxide formation. The oxide thickness can be calculated from the capacitance

$$d_{\text{ox}} = f_{\text{R}} \frac{\varepsilon_{\text{ox}} \varepsilon_0 A}{C_1} \quad (5)$$

where ε is the dielectric constant of the layer, A is the electrode area, f_{R} a roughness factor, and ε_0 the permittivity of vacuum. Using a value for $\varepsilon = 5.2$ (typical of anodic silicon dioxide²⁹) and $f_{\text{R}} = 1$, we estimate from the results shown in Figure 7 a thickness range of 6–9 nm. (These values are approximately a factor of 2 larger than those reported for Si by Bailes and co-workers, who used an ε value of 3.9 as for thermal oxide.¹⁸) The constant value of C_1 indicates a constant film thickness. However, the change in resistance suggests that the properties of the film are changing in time. The capacitance is determined by the ε/d ratio (eq 5); the individual parameters may be changing synchronously. Somewhat similar results are observed for the circuit elements Q_2 and R_2 : Q_2 shows a decrease by about 30% in time, whereas R_2 increases from 500 Ω at 5 min to 4700 Ω at 56 min.

The electrode rotation rate had a strong influence on the impedance plots. For example at 4 V in 0.033 M solution the radius of the Nyquist “semicircle” decreased by more than a factor of 2 as the rotation rate increased from 0 to 3000 rpm. Analysis of the results on the basis of the circuit used above showed that C_1 increased by 50%. This points to a decrease in the barrier layer thickness when mass transport is enhanced. The resistance R_1 decreased by a factor of 3 in the range 0 to 3000 rpm. Apart from a lower value at 0 rpm, Q_2 remains essentially independent of rotation rate. Like R_1 , R_2 decreases with increasing rotation rate also by a factor of 3. It is tempting to attribute this second circuit to the thick oxide seen in ellipsometry. In this case, R_2 would correspond to the resistance of this oxide. The origin of the CPE Q_2 is not clear. Viewed as a

capacitance, it has a value of the order of a Helmholtz capacitance (12–25 $\mu\text{F}/\text{cm}^2$).

4. Discussion

The results of this study point to an oxide layer with a duplex structure: an inner compact barrier layer (seen in impedance), and a thick permeable outer layer (ellipsometry, SEM, RBS). Such a combination of barrier and “porous” layers is common in anodic oxidation of semiconductors and metals; examples include Si,^{18,30} Al^{31,32} and Ti.³³ For SiC, the total oxide thickness can be extremely large (up to 5 μm). This is more than 3 orders of magnitude larger than that of the oxide formed on Si under similar conditions. The effect of hydrodynamics on the optical and impedance results provides evidence for a coupling of the two layers: enhanced mass transport decreases the steady-state total oxide thickness by enhancing the oxide etch rate, whereas the impedance results show that the barrier oxide becomes thinner (C_1 increases and R_1 decreases) with increasing electrode rotation rate. There is evidence from impedance measurements for a similar coupling of “dry” and “wet” anodic oxides in the case of Si.²⁸

Formation of the “dry” oxide will very likely be due to ionic transport driven by the electric field across the barrier layer. This reaction (see eq 3a) requires water molecules and releases protons (and oxidized carbon atoms). At the outer edge of the barrier layer, dry oxide is converted to a wet (hydrated) oxide (Figure 8). To maintain the reactions, protons must migrate and/or diffuse across the thick oxide to solution. Similarly, H₂O molecules must diffuse from solution to the interface of the two oxides while the carbon product is transported in the opposite direction. The oxide dissolves chemically at the solution interface (see eq 4a); mass-transport control of this reaction at the surface can explain why we do not detect fluoride species, either reactants or products, in the oxide by ERD. The results show that this reaction is mass-transport-controlled. The steady-state oxide thickness is determined by the rate of electrochemical formation and the rate of chemical etching of the oxide. The location at which barrier layer formation occurs on metals and semiconductors depends on which ionic species migrates through the solid. If O²⁻ (or OH⁻) ion migration is dominant, the layer grows at the substrate/oxide interface, whereas cation migration will give film formation at the outer edge of the barrier layer (Figure 8). For SiC, one expects the former on the basis of the results for Si.³⁴

An intriguing aspect of these results is the rapid conversion of dry to wet oxide giving rise to micrometer-thick

- (27) Ozanam, F.; Chazalviel, J. N.; Radi, A.; Etman, M. *J. Electrochem. Soc.* **1992**, *139*, 2491.
 (28) Serre, C.; Barret, S.; Herino, R. *J. Electrochem. Soc.* **1994**, *141*, 2049.
 (29) Schmuki, P.; Bohni, H.; Bardwell, J. A. *J. Electrochem. Soc.* **1995**, *142*, 1705.

- (30) Frey, S.; Keipert, S.; Chazalviel, J. N.; Ozanam, F.; Carstensen, J.; Föll, H. *Phys. Status Solidi A* **2007**, *204*, 1250.
 (31) Jessensky, O.; Müller, F.; Gosele, U. *J. Electrochem. Soc.* **1998**, *145*, 3735.
 (32) Masuda, H.; Hasegawa, F.; Ono, S. *J. Electrochem. Soc.* **1997**, *144*, L127.
 (33) Macak, J. M.; Albu, S.; Kim, D. H.; Paramasivam, I.; Aldabergerova, S.; Schmuki, P. *Electrochem. Solid-State Lett.* **2007**, *10*, K28.
 (34) Lehmann, V. *Electrochemistry of Silicon*; Wiley-VCH Verlag GmbH: Weinheim, Germany, 2002.

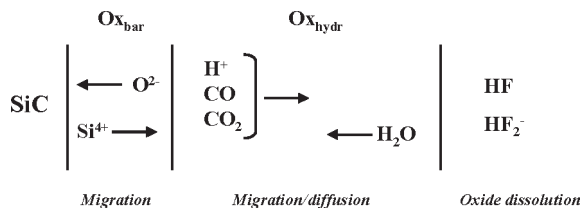


Figure 8. Schematic representation of the formation of a surface layer on SiC consisting of a barrier oxide (Ox_{bar}) with, on top, a hydrated oxide (Ox_{hydr}).

layers. What is involved in this reaction is not clear. It is unlikely that fluoride species are important. Very little fluoride is detected in the layer, whereas the photoanodic experiments of Rysy et al. with n-type 4H-SiC in 0.2 M HCl solution shows that thick oxide growth is not restricted to fluoride medium.²³ For Si, Böhm et al.³⁵ suggest that localized breakdown of the inner oxide, due to the high electric field, may be responsible for growth of the outer oxide. It has been suggested that mechanical stress in oxide plays an important role in the transition from barrier to porous layers.^{36,37} Chemistry may also be important. Anodic oxidation of SiC produces protons (eq 4b) whose concentration builds up at the outer edge of the dry oxide. This may lead to a weakening of the Si–O bonds,³⁰ which combined with the presence of gas molecules leads to less-dense oxide. If, as suggested, oxidation takes place at the semiconductor/oxide interface, the gaseous carbon product must then pass through the inner oxide. That gas molecules can be transported through a compact oxide is shown in work on group III-nitrides. Rotter and co-workers produced a gate dielectric for MOSFET devices by photoanodic oxidation of part of a 30 nm layer of n-type $\text{Al}_{0.2}\text{Ga}_{0.8}\text{N}$ in dilute alkaline solution.^{38–40} This is a 3-hole reaction and N_2 has to be released. This group has shown that thick oxide (up to 1.2 μm) can be grown on n-type GaN under comparable conditions.⁴¹ Our results suggest that such an oxide is likely to have a duplex structure.

The high oxidation rates observed for SiC electrodes covered with thick oxide imply a high permeability for ions and molecules and, consequently, a considerable degree of porosity. (Porosity could not be observed directly in our SEM experiments.) One way to get an indication of the compactness of the outer oxide layer is to compare the “optical” thickness with that expected from

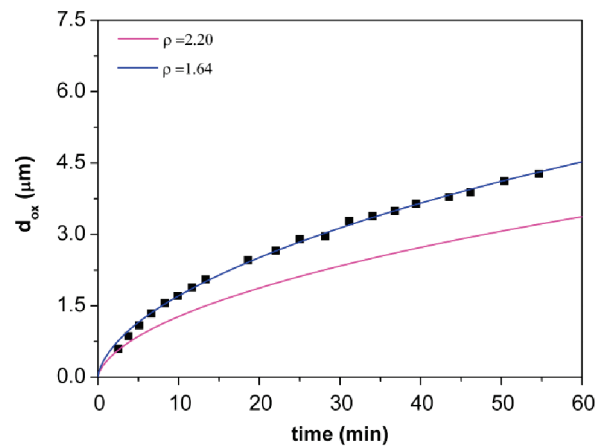


Figure 9. Solid squares show the measured oxide thickness as a function of growth time in 0.033 M fluoride solution at 4.5 V (see Figure 6). The solid lines give the thickness calculated on the basis of the charge passed for two oxide densities.

the charge passed during oxide formation. The latter depends on the oxidation valence, i.e., the number of charge carriers required to oxidize one formula unit of SiC and on the density of the oxide. (The oxidation valence is 4 for the case in which C in SiC is not oxidized, 6 for the case in which CO is formed, and 8 for CO_2 .) Figure 9 shows the oxide thickness determined from ellipsometry as a function of growth time. If we assume that CO and CO_2 are produced in equal amounts ($n = 7$), as found by Lauerman et al.,⁴² the best fit was obtained for a density of 1.64 g/cm^3 . This is considerably lower than that of compact thermal oxide (2.2 g/cm^3). Rysy et al. suggest a density of 1.65 g/cm^3 for the oxide grown in HCl solution.²³ The quality of the oxide produced in this work seems superior to that of the oxide grown in HCl solution.

Frey and co-workers have reported surprising results⁴³ for anodic oxide formation on Si in neutral or weakly alkaline fluoride solution at high potential (≥ 20 V). In this case, a duplex oxide is also formed but the outer oxide is much thicker than that observed at low potential in acidic fluoride solution. In addition, a strong self-ordering of the oxide morphology is observed. It would be interesting to see if analogous results are found with SiC under comparable conditions.

These results suggest that the thick porous layers formed on SiC might be interesting as semipermeable membranes for microelectromechanical systems (MEMS). Free-standing layers could be formed by complete anodic oxidation of thin SiC layers on Si. The membrane is released by anisotropic chemical etching of the Si substrate. A simple electrochemical method can be used to detect the point at which Si is completely removed.⁴⁴ This is necessary to prevent dissolution

(35) Böhm, S.; Peter, L. M.; Schlichthorl, G.; Greef, R. *J. Electroanal. Chem.* **2001**, *500*, 178.

(36) Houser, J. E.; Hebert, K. R. *Nat. Mater.* **2009**, *8*, 415.

(37) Jessensky, O.; Müller, F.; Gösele, U. *Appl. Phys. Lett.* **1998**, *72*, 1173.

(38) Rotter, T.; Mistele, D.; Stemmer, J.; Seyboth, M.; Schwegler, V.; Paprotta, S.; Fedler, F.; Klausling, H.; Semchinova, O. K.; Aderhold, J.; Graul, J. *Electron. Lett.* **2001**, *37*, 715.

(39) Mistele, D.; Rotter, T.; Rover, K. S.; Paprotta, S.; Seyboth, M.; Schwegler, V.; Fedler, F.; Klausling, H.; Semchinova, O. K.; Stemmer, J.; Aderhold, J.; Graul, J. *Mater. Sci. Eng., B* **2002**, *93*, 107.

(40) Rotter, T.; Ferretti, R.; Mistele, D.; Fedler, F.; Klausling, H.; Stemmer, J.; Semchinova, O. K.; Aderhold, J.; Graul, J. *J. Cryst. Growth* **2001**, *230*, 602.

(41) Rotter, T.; Mistele, D.; Stemmer, J.; Fedler, F.; Aderhold, J.; Graul, J.; Schwegler, V.; Kirchner, C.; Kamp, M.; Heuken, M. *Appl. Phys. Lett.* **2000**, *76*, 3923.

(42) Lauerman, I.; Meissner, D.; Reineke, R. *DEHEMA. Monogr.* **1991**, *124*, 617.

(43) Frey, S.; Gesillon, B.; Ozanam, F.; Chazalviel, J. N.; Carstensen, J.; Foll, H.; Wehrspohn, R. B. *Electrochem. Solid-State Lett.* **2005**, *8*, B25.

(44) Philipsen, H. G. G.; Smeenk, N. J.; Ligthart, H.; Kelly, J. J. *Electrochem. Solid-State Lett.* **2006**, *9*, C118.

of the relatively reactive oxide layer. Alternatively, the work of Rotter et al.^{38–40} on GaN and AlGaIn suggests that (photo)anodic oxidation might be an interesting approach to making dielectric oxide on SiC (possibly with a low density of interface states) for device applications.

5. Summary and Conclusions

Anodic polarization of 4H and 6H SiC in dilute fluoride solution at pH 3 gives rise to the growth of silicon dioxide layers with a thickness up to at least 5 μm at relatively high current densities. Valence-band holes are essential for the electrochemical reaction. Gas evolution is observed during layer growth. The oxide was characterized by SEM, RBS, and ERD. Very little carbon was observed in the layer in ERD experiments. This supports the idea that carbon is oxidized to CO and CO₂, which are removed from the layer by the high vacuum during the ERD experiment. In-situ potential step, electrical impedance and spectroscopic ellipsometry measurements were used to study the kinetics of anodic growth and chemical

dissolution of the oxide. The results indicate the formation of a duplex layer: a thin inner “dry” oxide film and a thick outer porous layer of “hydrated” oxide (in analogy to anodic oxide on silicon). The results suggest that these layers are “coupled”. Surprisingly, the oxide grown on SiC has a thickness more than 3 orders of magnitude larger than that formed on Si under comparable conditions. The oxide on SiC must be porous to allow transport of H⁺, H₂O and CO/CO₂ and thus account for the high current densities observed. The huge difference in oxide thickness on the two semiconductors is attributed to the presence of carbon in the compound semiconductor: C must be removed from the lattice to allow oxide growth (formation of Si–O–Si bonds), whereas the evolution of CO and CO₂ is certain to influence the oxide morphology and transport properties.

Acknowledgment. The authors thank Ruud Balkenende of Philips Research for the useful discussions and Hans Ligthart and Rinus Mackaay for technical assistance. This work was financially supported by the Dutch Technology Foundation (STW, UPC-6317).